Theor Chem Acc (2010) 125:65–73
DOI 10.1007/s00214-009-0663-4

REGULAR ARTICLE

CASPT2 and CASSCF studies on the low-lying electronic states of the HCCO radical and its anion

Yue-Jie Liu · Zeng-Xia Zhao · Hong-Xing Zhang · Chia-Chung Sun

Received: 20 August 2009 / Accepted: 15 October 2009 / Published online: 6 November 2009

Abstract The complete active space self-consistent field and multiconfigurational second-order perturbation theory methods have been used to investigate the low-lying electronic states of the HCCO radical and its anion. The calculated geometrical structure and harmonic vibrational frequencies for the X^2A'' state of HCCO are in good agreement with experimental values. The barrier to $1^2\Pi$ ($1^2A'$) is estimated to be 0.069 eV (554 cm^{-1}), which is also close to experimental result (540 cm^{-1}). Moreover, we find that the $2^2A'$ state is bent, while $2^2\Pi$ ($2^2A''$) is linear. By comparing the oscillator strengths and adiabatic excitation energies, we show that the $2^2\Pi$ ($2^2A''$) ← X^2A'' transition is the most intense among these transitions. The unpaired electrons mainly locate on the C atoms in the $2^2A'$ and $2^2\Pi$ ($2^2A''$) states according to the Mulliken spin populations. On the other hand, for $HCCO^-$, the first adiabatic and vertical detachment energies are 2.210 and 2.362 eV, respectively, which reasonably agree with experimental value of 2.338 ± 0.008 eV. Remarkably, we explore several higher excited states of the HCCO radical ($1^4A'$, $2^4A''$ and *cis*-$1^4A'$) and its anion ($1^3A''$, $1^1A''$ and $1^3A'$), which have not been reported in previous studies.

Keywords HCCO · Excited state · CASSCF · CASPT2

Electronic supplementary material The online version of this article (doi:10.1007/s00214-009-0663-4) contains supplementary material, which is available to authorized users.

Y.-J. Liu · Z.-X. Zhao · H.-X. Zhang (✉) · C.-C. Sun
State Key Laboratory of Theoretical and Computational Chemistry, Institute of Theoretical Chemistry, Jilin University, 130023 Changchun, People's Republic of China
e-mail: zhanghx@jlu.edu.cn

1 Introduction

The ketenyl radical (HCCO) is a critical intermediate in the oxidation of acetylene that often takes place in the process of hydrocarbon combustion [1–4]. Therefore, many studies have been reported to characterize the spectroscopy and kinetics of HCCO [5–14]. Experimentally, Endo et al. observed the pure rotational spectrum of the HCCO radical [5, 6]. They showed that the ground state of HCCO has a planar and quasilinear structure in the submillimeter-wave region. The electronic transition of $2^2\Pi \leftarrow X^2A''$ was firstly presented at 4.14 eV through the photodissociation spectroscopy [7, 8]. Subsequently, Brock et al. studied the same band via the laser induced fluorescence (LIF) [9, 10]. For the ground state of HCCO, the modes of ν_1 CH stretch, ν_2 asymmetric CCO stretch, ν_5 CCH (*cis*) bending were found to be 3,232, 2,023 and 494 cm^{-1} [9, 11, 12], respectively. Additionally, in 2001, Schäfer et al. reported that the electron affinity of HCCO was 2.338 ± 0.008 eV [13], which further testified the previous experimental result (2.350 ± 0.020 eV) [14]. They presented the photoelectron spectrum of the $HCCO^-$ anion at the photodetachment wavelength of 355 nm.

Theoretically [15–26], it is known that the $1^2\Pi$ state of HCCO is split to form the bent X^2A'' state and linear $1^2A'$ state due to the Renner–Teller (R–T) effect [15–17]. The calculated barrier to the linear $1^2A'$ state of radical was 643 cm^{-1} by Szalay and co-workers [18]. In 2005, they further explored the equilibrium geometries and frequencies for the X^2A'' state of HCCO at the CCSD(T)/(aug)cc-pVnZ ($n = T, Q$) levels [21]. Moreover, Schäfer et al. studied the vibronic spectrum of HCCO involving the X^2A'' state and first low-lying excited state [13]. Sattelmeyer et al. characterized the X^2A'' state of HCCO and its four low-lying isomers, which were found to be minima [20, 23].

The second doublet excited state of the HCCO radical received much attention and was assigned as a doubly degenerate linear state ($2^2\Pi$) in the spectroscopic experiments [8, 9]. However, Brock et al. thought that the second R–T pair produced two nonlinear minima, which provided a reasonable description of the four bending potentials for the $2^2\Pi$ state [10]. Thus, in the present work, we investigate the low-lying electronic states of the HCCO radical and its anion through the CASSCF and CASPT2 methods. The two calculation methods have been successfully employed in the previous studies of electronic excited states and are shown to be enough accurate [27–37]. On the basis of the calculations, we suggest that one of the second R–T pair of HCCO is linear, while the other is nonlinear. Moreover, the analyses of the spin populations indicate that the radical mainly originates from the contribution of the C atom in the $2^2\Pi$ state, which is different from previous report of an oxygen-based radical [10]. Considering the importance of the photoelectron spectrum, we further explore the adiabatic detachment energies (ADE) and vertical detachment energies (VDE) of $HCCO^-$.

2 Calculation details

The complete active space (CAS) SCF [34, 35] method was used to generate molecular orbitals and reference functions for subsequent multiconfigurational second-order perturbation theory (CASPT2) [36, 37] calculations. Based on the previous experimental and theoretical studies [5–10, 18–22], the planar structure with C*s* symmetry was adopted to obtain the electronic excited states. With the cc-pVTZ basis set [38], the equilibrium geometries of every state were obtained by using the CASPT2 and CASSCF optimization methods [30–33], respectively. To examine the effects of the basis sets in our results, we also employed the CASSCF method with the ANO-L basis set [39, 40] to optimize the geometries. Furthermore, the CASPT2 program was used to compute the corresponding dynamic correction energies. We calculated the harmonic vibrational frequencies at the CASSCF/ANO-L level by employing multiconfigurational linear response (MCLR) [41]. The oscillator strengths were computed by the CASSCF state interaction (CASSI) program [42] with the CASPT2 energy differences.

As is known, how to select an active space is crucial for obtaining accurate results. By performing a HF calculation for $HCCO^-$, we obtained the orbitals in order of increasing energy (core)$(4a')^2(5a')^2(6a')^2(7a')^2(1a'')^2(8a')^2(9a')^2(2a'')^2(10a')^0(11a')^0$ $(12a')^0(13a')^0(3a'')^0$, in which the core represents $(1a')^2(2a')^2(3a')^2$. The 4a′ orbital was composed of the 2s orbital of O atom and the energy gap between 4a′ and 5a′ was more than 8 eV. To keep a balance between cost and precision in the computations, both the core orbitals and the 2s orbital of O atom were treated as inactive. Thus, we chose 13 active electrons and 12 active orbitals (from 5a′ to 3a″) for the HCCO radical, and 14 active electrons with the same active orbitals for $HCCO^-$.

All calculations were carried out with the MOLCAS 6.2 quantum-chemistry software [43]. For the CASPT2 calculations in the present work, the weight values of the CASSCF reference functions in the first-order wave functions were larger than 80%, unless otherwise noted.

3 Results and discussion

3.1 HCCO

3.1.1 Geometries

Firstly, we study the geometrical structures of the ground state and low-lying excited states of the HCCO radical at CASPT2/cc-pVTZ, CASSCF/cc-pVTZ and CASSCF/ANO-L levels, respectively. The obtained structural parameters are shown in Table 1 through various methods or basis sets.

It is known that the ground state X^2A'' and first low-lying excited state $1^2\Pi$ ($1^2A'$) are the two components of the R–T pair [15–17]. Thus, we firstly elucidate the geometry of the X^2A'' state. As shown in Fig. 1, the X^2A'' state is a *trans*-bent planar structure, which has been reported by previous studies [5, 6, 18–22]. For the X^2A'' state, we find that there are no obvious differences in the equilibrium geometries through CASSCF method with the cc-pVTZ and ANO-L basis sets as shown in Table 1. However, the differences in equilibrium geometries through CASSCF and CASPT2 methods are apparent.

In detailed, the obtained bond length of C–H through CASSCF method is 1.085 Å, which is slightly larger than that of CASPT2 method (1.067 Å). We should point out that the latter is closer to the experimental value ($r_0 = 1.056$ Å) [5]. Through CASSCF and CASPT2 methods, the bond lengths of C–C are 1.320 and 1.294 Å, respectively, which are in agreement with the previous investigations [13, 18–22]. Moreover, the C–O bond lengths are 1.174 and 1.178 Å at CASSCF/cc-pVTZ and CASPT2/cc-pVTZ levels, respectively. The sum of the C–C and C–O bond lengths at CASPT2/cc-pVTZ level is 2.472 Å, which is close to the reported value of Endo et al. (2.464 Å) [5].

On the other hand, the calculated bond angles of HCC are 130.6° and 136.8° at the CASSCF/cc-pVTZ and CASPT2/cc-pVTZ levels, respectively. It is found that the latter is in better agreement with previous experiment

Table 1 Equilibrium geometries (bond length (r_e) in Å and bond angle (θ) in °) and adiabatic excitation energies (T_0 in eV) of the ground state and low-lying excited states of HCCO[a]

State	Method/basis set	$r_{e(C-H)}$	$r_{e(C-C)}$	$r_{e(C-O)}$	$\theta_{(HCC)}$	$\theta_{(CCO)}$	T_0 (CASSCF)	T_0 (CASPT2)
X^2A''	CASPT2/cc-pVTZ	1.067	1.294	1.178	136.8	169.4	0.000	0.000
	CASSCF/cc-pVTZ	1.085	1.320	1.174	130.6	167.3	0.000	0.000
	CASSCF/ANO-L	1.085	1.320	1.171	130.2	167.4	0.000	0.000
	Expt[b]	1.056			138.7			
	CCSD(T)/cc-pVTZ[c]	1.066	1.297	1.173	134.6	169.4		
	CCSD(T)/cc-pVQZ[d]	1.069	1.297	1.170	134.1	169.4		
	B3LYP/cc-pVQZ[e]	1.070	1.287	1.170	137.3	170.8		
$1^2\Pi$ ($1^2A'$)	CASPT2/cc-pVTZ	1.059	1.261	1.189			0.101	0.069
	CASSCF/cc-pVTZ	1.071	1.272	1.188			0.110	0.060
	CASSCF/ANO-L	1.071	1.272	1.186			0.109	0.031 (0.0003)[h]
	Expt[b]							0.067
	UHF-CCSD(T)/cc-pVTZ[c]	1.056	1.261	1.185				0.080
	CCSD(T)/cc-pwCVTZ[e]	1.060	1.256	1.181				0.067
$1^4A''$	CASPT2/cc-pVTZ	1.073	1.437	1.206	136.4	117.7	2.688	2.757
	CASSCF/cc-pVTZ	1.089	1.476	1.196	133.2	121.0	2.663	2.772
	CASSCF/ANO-L	1.067	1.459	1.191	131.4	122.2	2.360	2.804
	CCSD(T)/cc-pVQZ[f]	1.077	1.437	1.201	135.0	119.0		2.793
$2^2A'$	CASPT2/cc-pVTZ	1.065	1.263	1.339	145.8	169.2	4.308	4.019
	CASSCF/cc-pVTZ	1.082	1.281	1.341	139.7	166.8	4.304	4.021
	CASSCF/ANO-L	1.082	1.280	1.340	139.8	166.8	4.399	4.084 (0.0001)[h]
$2^2\Pi$ ($2^2A''$)	CASPT2/cc-pVTZ	1.058	1.252	1.340	180.0	179.9	4.374	4.054
	CASSCF/cc-pVTZ	1.072	1.264	1.341	179.8	179.9	4.381	4.048
	CASSCF/ANO-L	1.072	1.262	1.339	180.0	180.0	4.389	3.997 (0.0064)[h]
	Expt[g]							4.14
	EOM-IP/cc-pVTZ[c]	1.054	1.232	1.330				4.471
$1^4A'$	CASPT2/cc-pVTZ	1.070	1.464	1.209	137.0	174.4	5.084	4.990
	CASSCF/cc-pVTZ	1.087	1.508	1.212	129.8	175.9	5.051	5.004
	CASSCF/ANO-L	1.086	1.506	1.209	129.9	175.9	5.044	4.979
$2^4A''$	CASPT2/cc-pVTZ	1.080	1.366	1.405	121.5	125.1	6.447	6.086
	CASSCF/cc-pVTZ	1.097	1.386	1.420	121.0	124.0	6.449	6.085
	CASSCF/ANO-L	1.071	1.385	1.421	123.9	122.7	6.550	6.166
cis-$1^4A''$	CASPT2/cc-pVTZ	1.084	1.442	1.197	132.4	125.2	2.313	2.451
	CASSCF/cc-pVTZ	1.099	1.473	1.192	131.4	127.1	2.305	2.453
	CASSCF/ANO-L	1.074	1.477	1.194	130.8	126.2	2.284	2.517
	CCSD(T)/cc-pVQZ[f]	1.087	1.441	1.195	131.3	125.3		2.476
cis-$1^4A'$	CASPT2/cc-pVTZ	1.079	1.334	1.420	132.8	126.4	5.688	5.720
	CASSCF/cc-pVTZ	1.096	1.347	1.430	130.8	126.4	5.693	5.715
	CASSCF/ANO-L	1.095	1.346	1.429	130.8	126.3	5.704	5.723

[a] The CASSCF and CASPT2 energies for the ground state of HCCO are −151.3126559 and −151.6973056 au, −151.3132739 and −151.6966883 au, −151.3259841 and −151.8042166 au, respectively, at the levels of CASPT2/cc-pVTZ, CASSCF/cc-pVTZ and CASSCF/ANO-L

[b] The experimental values were taken from Ref. [5]

[c] The theoretical values were taken from Ref. [18]

[d] The theoretical values were taken from Ref. [21]

[e] The theoretical values were taken from Ref. [22]

[f] The theoretical values were taken from Ref. [20]

[g] The experimental value was taken from Ref. [7]

[h] The oscillator strengths of $1^2\Pi$ ($1^2A'$), $2^2A'$ and $2^2\Pi$ ($2^2A''$) are listed in parentheses, respectively

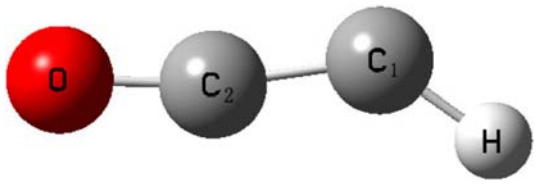

Fig. 1 Atom labels for the *trans*-HCCO radical (C*s* symmetry) used in the present work (the molecule lies in the XY plane)

(138.7°) [5]. Moreover, the bond angle of CCO (169.4°) with CASPT2 method is also consistent with the theoretical results at CCSD(T)/cc-pVnZ ($n = T, Q$) levels [18, 21]. As shown in Table 1, comparing with the CASSCF method, we find that the CASPT2 method makes an improvement in predicting the C–H bond length and the HCC bond angle in the present work. The calculated structural parameters of the X^2A'' state with CASPT2 method are in better agreement with the experimental results [5]. This is expected, because CASPT2 is an effective way to recover the dynamical correlation effects for the systems with π-electrons [31–33]. Thus, the CASPT2 geometries would be employed to discuss the subsequent results.

It is worth to mentioning that Szalay et al. studied the geometry of HCCO at CCSD(T)/cc-pVQZ level [21]. We find that the calculated geometrical parameters through CASPT2 method in our work are in good agreement with those of Szalay ($r_{e(C-H)} = 1.069$ Å, $r_{e(C-C)} = 1.297$ Å, $r_{e(C-O)} = 1.170$ Å, $\theta_{(HCC)} = 134.1°$, $\theta_{(CCO)} = 169.4°$). This further testifies that the CASPT2 method in the present work is enough accurate.

The leading configurations (the weights exceed 0.05) and configuration interaction (CI) coefficients for the electronic states of the HCCO radical are listed in Table 2. We find that the X^2A'' state has a dominant electronic configuration of $(\text{core})(4a')^2(5a')^2(6a')^2(7a')^2(8a')^2(1a'')^2(9a')^2(2a'')^\alpha$ with a coefficient of 0.9455. Moreover, Fig. 2 displays the plots of orbitals involved in the active space for the X^2A'' state. As shown in Fig. 2, the 8a′ orbital of X^2A'' is mainly composed of π (C_2–O) orbital, while the effects of σ (C_1–H) and σ (C_1–C_2) slightly contribute to the 8a′ orbital. The 9a′ orbital is a π* (π_{C1-C2}–Op_y) orbital (the interaction between π (C_1–C_2) bonding and π* (C_2–O) antibonding) in which the contribution of C_2 atom is small. We also find that the slight σ (C_1–C_2) effect contributes to the 9a′ orbital. It is evident that the 10a′ orbital is a π* (C_1–C_2–O) orbital. Moreover, the 1a″, 2a″, and 3a″ orbitals of X^2A'' are all constituted by the p_z orbital. It can be seen from Fig. 2 that the three orbitals are assigned as π (C_2–O) orbital, π* (π_{C1-C2}–Op_z) orbital and π* (C_1–C_2–O) orbital, respectively.

The single electron transition from the 9a′ orbital to the 2a″ orbital forms the $1^2\Pi$ ($1^2A'$) state. Furthermore, the

Table 2 Leading configurations (the weights exceed 5%) and CI coefficients in the CASSCF calculations for the electronic states of HCCO[a]

State	Coef	Configuration
X^2A''	0.9455	$(8a')^2(1a'')^2(9a')^2(2a'')^\alpha$
$1^2\Pi$ ($1^2A'$)	0.9470	$(1\pi_y)^2(1\pi_z)^2(2\pi_z)^2(2\pi_y)^\alpha$
$1^4A''$	0.9581	$(8a')^2(1a'')^2(9a')^\alpha(2a'')^\alpha(10a')^\alpha$
$2^2A'$	−0.8527	$(8a')^\alpha(1a'')^2(9a')^2(2a'')^2$
	−0.3013	$(8a')^2(1a'')^2(2a'')^2(10a')^\alpha$
$2^2\Pi$ ($2^2A''$)	−0.8806	$(1\pi_y)^2(1\pi_z)^\alpha(2\pi_z)^2(2\pi_y)^2$
	0.2486	$(8a')^2(1a'')^2(9a')^2(3a'')^\alpha$
$1^4A'$	−0.9526	$(8a')^2(1a'')^2(9a')^\alpha(2a'')^\alpha(3a'')^\alpha$
$2^4A''$	−0.7009	$(8a')^\alpha(1a'')^2(9a')^2(2a'')^\alpha(10a')^\alpha$
	−0.5791	$(8a')^2(1a'')^\alpha(9a')^\alpha(2a'')^2(10a')^\alpha$
cis-$1^4A''$	0.9596	$(8a')^2(1a'')^2(9a')^\alpha(2a'')^\alpha(10a')^\alpha$
cis-$1^4A'$	0.9359	$(8a')^\alpha(1a'')^2(9a')^\alpha(2a'')^2(10a')^\alpha$

[a] The common configuration $(\text{core})(4a')^2(5a')^2(6a')^2(7a')^2$ is not presented for X^2A'', $1^4A''$, $2^2A'$, $1^4A'$, $2^4A''$, *cis*-$1^4A''$ and *cis*-$1^4A'$. The common configuration $(\text{core})(4\sigma)^2(5\sigma)^2(6\sigma)^2(7\sigma)^2$ is not presented for $1^2\Pi$ ($1^2A'$) and $2^2\Pi$ ($2^2A''$). In active orbitals the number '2' represents a fully occupied orbital, and 'α' represents a singly occupied orbital containing an electron with an up spin

electronic configuration can be described as $(\text{core})(4\sigma)^2(5\sigma)^2(6\sigma)^2(7\sigma)^2(1\pi_y)^2(1\pi_z)^2(2\pi_z)^2(2\pi_y)^\alpha$ with a coefficient of 0.9470. The plots of orbitals included in the active space for the $1^2\Pi$ ($1^2A'$) state are presented in Fig. 3. Comparing with the X^2A'' state, we find that the bond lengths of $1^2\Pi$ ($1^2A'$) change as follows: the C–C and C–H bond lengths decrease to 1.261 and 1.059 Å, respectively, whereas the C–O bond length increases to 1.189 Å. The electron transition enhances the effects of π (C_1–C_2) bonding and π* (C_2–O) antibonding, thus making the C–C bond shorter and the C–O bond longer than those of X^2A''.

One electron in the 9a′ orbital is promoted to the 10a′ or 3a″ orbital, resulting in the formation of the $1^4A''$ or $1^4A'$ state. We find that the two formed states exhibit the single-reference character as shown in Table 2. The electron transition from the π* (π_{C1-C2}–Op_z) orbital to the π* (C_1–C_2–O) orbital makes the C–C and C–O bonds prolonged. For the $1^4A''$ and $1^4A'$ states, the C–C bond lengths increase to 1.437 and 1.464 Å, and the C–O bond lengths increase to 1.206 and 1.209 Å, respectively. As can be seen in Table 1, the obtained geometrical parameters of the $1^4A''$ state with CASPT2 method are consistent with previous report at the CCSD(T)/cc-pVQZ level [20].

As shown in Table 2, the $2^2A'$ and $2^2\Pi$ ($2^2A''$) states have obvious multiconfigurational character. Here, we firstly analyze the dominant electron configurations with the coefficients of −0.8527 and −0.8806, respectively. The two states mainly originate from the electron transition from the π (C_2–O) orbital to the π* (π_{C1-C2}–Op_z) orbital

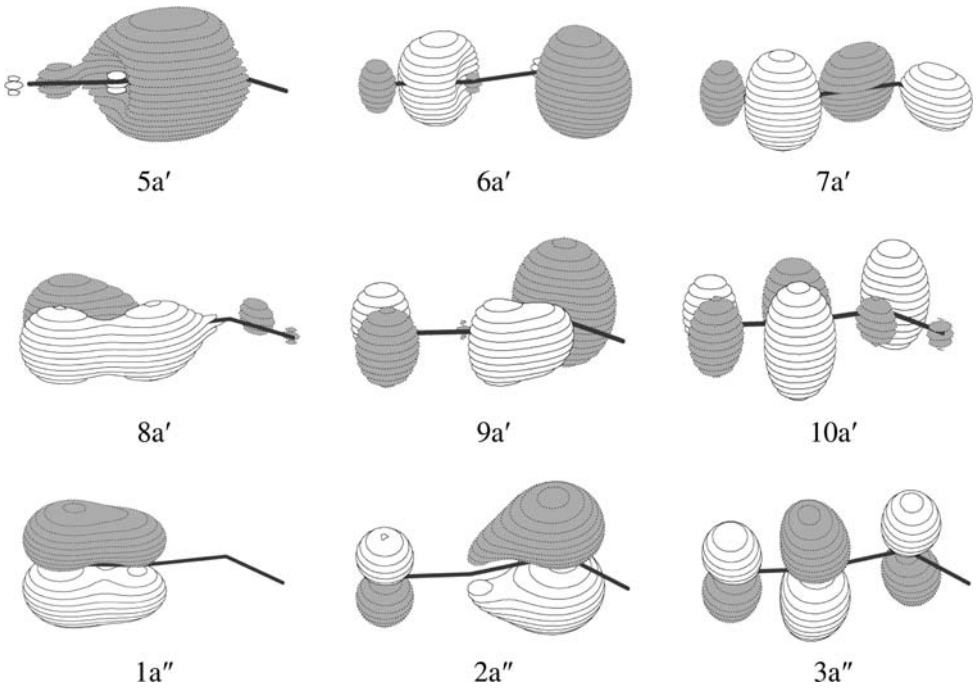

Fig. 2 The plots of orbitals included in the active space for the ground state of HCCO (visualization using the MOLDEN program)

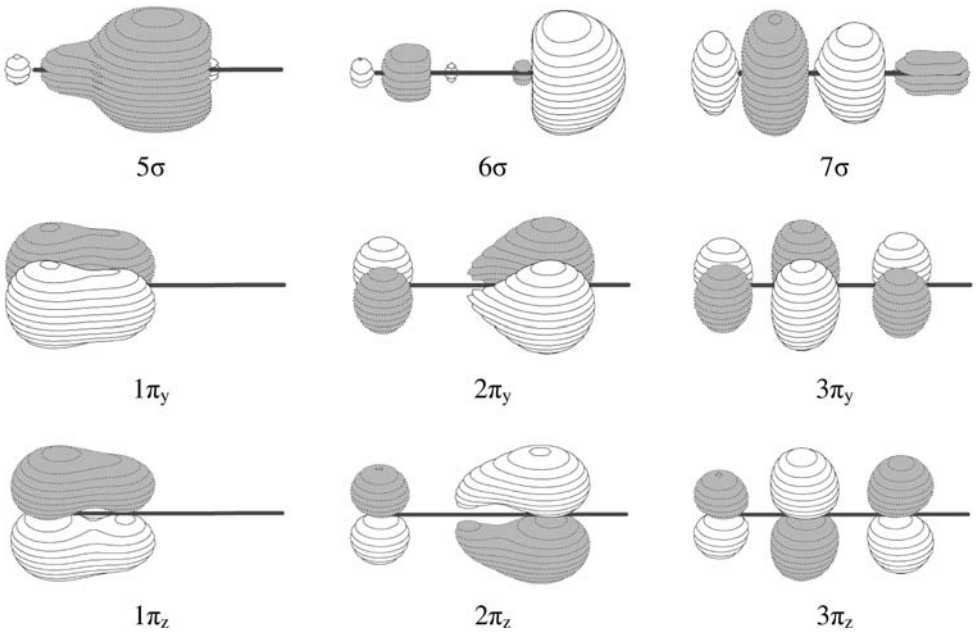

Fig. 3 The plots of orbitals included in the active space for the $1^2\Pi$ ($1^2A'$) state of HCCO (visualization using the MOLDEN program)

(from 8a′ or 1a″ to 2a″). Compared with the ground state, the C–C bond lengths of the two states decrease to 1.263 ($2^2A'$) and 1.252 Å ($2^2A''$), while the C–O bond increase to 1.339 ($2^2A'$) and 1.340 Å ($2^2A''$), respectively, as shown in Table 1. Moreover, the HCC bond angle (145.8°) in the $2^2A'$ state is larger than that of X^2A'' (136.8°). This is because the $2^2A'$ state has the character of −0.3013 (9a′ → 2a″, 10a′), and this component reduces the in-plane electrons at C_1 atom which withdraw the C_1 nucleus. Additionally, we find that the CCO bond angle of the $2^2A'$ state still remains 169.2°.

Remarkably, previous studies have shown that the $2^2\Pi$ ($2^2A''$) state is an oxygen-based radical with a C–C triple bond [10]. However, we find that the radical in the $2^2\Pi$ ($2^2A''$) state mainly locates on C_2 atom without forming the C–C triple bond. In detailed, (i) the C–C bond length of $2^2\Pi$ ($2^2A''$) obtained by the CASPT2 method is 1.252 Å, which is intervenient between the C–C double bond (1.34 Å) and C–C triple bond (1.20 Å). (ii) As shown in supporting information (Table S1), the CASSCF Mulliken spin populations of C_1 and O atoms in X^2A'' are 0.7886 and 0.2244, respectively. The value of 0.7886 indicates that the

radical lies on the C_1 atom for the X^2A'' state. For the $2^2\Pi$ ($2^2A''$) state, the spin population of C_2 atom (0.6574) is drastically larger than that of O atom (0.3282). Therefore, the radical mainly comes from the contribution of C_2 atom. The CASSCF Mulliken spin populations of the $2^2A'$ state are similar to those of the $2^2\Pi$ ($2^2A''$) state, thus we do not discuss repeatedly.

The $2^4A''$ state has obvious multiconfigurational character: the electronic configuration (i) (core)$(4a')^2(5a')^2(6a')^2(7a')^2(8a')^{\alpha}(1a'')^2(9a')^2(2a'')^{\alpha}(10a')^{\alpha}$ with a coefficient of −0.7009, and (ii) (core)$(4a')^2(5a')^2(6a')^2(7a')^2(8a')^2(1a'')^{\alpha}(9a')^{\alpha}(2a'')^2(10a')^{\alpha}$ with a coefficient of −0.5791. The former indicates that the electron is promoted from 8a′ to 10a′, while the transitions from 9a′ and 1a″ to 10a′ and 2a″ are observed in the latter. These transitions make the C–C and C–O bond lengths increase to 1.366 and 1.405 Å, respectively, as shown in Table 1.

Both the *cis*-$1^4A''$ state and the *cis*-$1^4A'$ state present the single-reference character. The transition process of the *cis*-$1^4A''$ state is similar to that of the $1^4A''$ state, thus the corresponding optimized equilibrium geometries are also similar. Moreover, the obtained geometry of *cis*-$1^4A''$ in our work is coincident with previous report at the CCSD(T)/cc-pVQZ level [20]. Additionally, the *cis*-$1^4A'$ state is the results of double excitations (8a′ → 10a′ and 9a′ → 2a″), which make the C–C and C–O bonds increase to 1.334 and 1.420 Å, respectively.

The harmonic vibrational frequencies for the low-lying electronic states of the HCCO radical are listed in Table 3. For the ground state X^2A'', the ν_1 CH stretch (3,213 cm^{-1}), ν_2 asymmetric CCO stretch (2,059 cm^{-1}) and ν_5 CCH (*cis*) bending (504 cm^{-1}) modes agree with experimental values of 3,232, 2,023 and 494 cm^{-1} [9, 11, 12]. Furthermore, the calculated ν_3 symmetric CCO stretch, ν_4 CCO (*trans*) bending and ν_6 CCO out-of-plane bending modes of X^2A'' are 1,196, 579 and 494 cm^{-1} in the present work, respectively. The calculated harmonic vibrational frequencies of X^2A'' in the present work are in agreement with those of Szalay's reports ($\nu_1 = 3{,}352\ cm^{-1}$, $\nu_2 = 2{,}097\ cm^{-1}$, $\nu_3 = 1{,}246\ cm^{-1}$, $\nu_4 = 567\ cm^{-1}$, $\nu_5 = 505\ cm^{-1}$, $\nu_6 = 500\ cm^{-1}$) [21]. Compared with the harmonic vibrational frequencies of the X^2A'' state, the values of ν_1, ν_2, and ν_3 of $1^2\Pi$ ($1^2A'$) are increased. It is found that the $1^2\Pi$ ($1^2A'$) state has one imaginary frequency 297i along the CCH out-of-plane bending. Moreover, the frequencies of the $2^2A'$ state show that it is a stable state. Because the $2^2\Pi$ ($2^2A''$) state has not convergent frequencies in a″ symmetry, we only list the frequencies of the a′ symmetry.

Table 3 Harmonic vibrational frequencies for the low-lying electronic states of HCCO calculated with the optimized geometries at CASSCF/ANO-L level[a]

State	ν_1(a′)	ν_2(a′)	ν_3(a′)	ν_4(a′)	ν_5(a′)	ν_6(a″)	ν_7(a″)
X^2A''	3,213	2,059	1,196	579	504	494	
Expt.	3,232[b]	2,023[c]			494[d]		
Ref[e]	3,352	2,097	1,246	567	505	500	
$1^2\Pi$ ($1^2A'$)	3,364	2,080	1,276	518	301	602	297i
$1^4A''$	3,375	1,822	1,133	506	923	358	
$2^2A'$	3,501	2,158	1,043	374	567	406	
$2^2\Pi$ ($2^2A''$)	3,390	2,201	1,045	148	484		
$1^4A'$	3,184	1,920	865	316	917	349	
$2^4A''$	3,356	1,388	1,089	514	856	555	
cis-$1^4A''$	3,307	1,796	1,032	493	992	624	
cis-$1^4A'$	3,090	1,545	989	432	893	547	

[a] ν_1(a′) denotes CH stretch, ν_2(a′) denotes asymmetric CCO stretch, ν_3(a′) denotes symmetric CCO stretch, ν_4(a′) denotes CCO (*trans*) bending, ν_5(a′) denotes CCH (*cis*) bending, ν_6(a″) denotes CCO out-of-plane bending, ν_7(a″) denotes CCH out-of-plane bending mode of the $1^2\Pi$ ($1^2A'$) state

The harmonic vibrational frequencies are in cm^{-1}

[b] The experimental value was taken from Ref. [11]

[c] The experimental value was taken from Ref. [12]

[d] The experimental value was taken from Ref. [9]

[e] The theoretical values were taken from Ref. [21]

3.1.2 The adiabatic excitation energies

On the basis of the stable geometries at CASPT2/cc-pVTZ, CASSCF/cc-pVTZ and CASSCF/ANO-L levels, respectively, we calculated the corresponding adiabatic excitation energies (T_0) by using CASSCF and CASPT2 methods as displayed in Table 1. Comparing the energetic values of CASSCF and CASPT2 suggested that the dynamical electron correlation effects must be considered in calculations. By using the method of CCSD(T), Szalay et al. and Jerosimić have independently demonstrated that the barriers to the $1^2\Pi$ ($1^2A'$) state are 643 and 544 cm^{-1}, respectively [18, 22]. However, the obtained barrier in our work is 0.069 eV (554 cm^{-1}) through CASPT2//CASPT2 method, which well agrees with the spectral experiment (540 cm^{-1}) [5].

One of the most important results from Table 1 is that the values of T_0 are dependent on the employed basis sets. At the CASPT2/cc-pVTZ and CASSCF/cc-pVTZ levels, the T_0 (CASPT2) values of $2^2A'$ are lower by 0.035 and 0.027 eV than those of $2^2\Pi$ ($2^2A''$), respectively. At the CASSCF/ANO-L level, however, T_0 (CASPT2) of $2^2A'$ is larger by 0.087 eV than that of $2^2\Pi$ ($2^2A''$). The CASPT2//CASPT2 T_0 value of $2^2\Pi$ ($2^2A''$) is 4.054 eV, which is close to experimental value of 4.14 eV [7]. Therefore, for the two states, we found that the T_0 (CASPT2) values at the CASPT2/cc-pVTZ level are more reliable than those of the CASSCF/ANO-L level. The oscillator strengths of $1^2\Pi$ ($1^2A'$), $2^2A'$ and $2^2\Pi$ ($2^2A''$) are 0.0003, 0.0001 and 0.0064,

Table 4 Equilibrium geometries (bond length (r_e) in Å and bond angle (θ) in °) and adiabatic excitation energies (T_0 in eV) of the ground state and low-lying excited states of $HCCO^-$[a]

State	Method/basis set	$r_{e(C-H)}$	$r_{e(C-C)}$	$r_{e(C-O)}$	$\theta_{(HCC)}$	$\theta_{(CCO)}$	T_0 (CASSCF)	T_0 (CASPT2)
X^1A'	CASPT2/cc-pVTZ	1.065	1.260	1.227	140.7	172.6	0.000	0.000
	CASSCF/cc-pVTZ	1.085	1.278	1.225	133.7	171.1	0.000	0.000
	CASSCF/ANO-L	1.084	1.279	1.222	133.8	171.2	0.000	0.000
	CCSD(T)/aug-cc-pCVQZ[b]	1.070	1.264	1.222	138.5	171.1		
Σ^+	CASPT2/cc-pVTZ	1.055	1.241	1.234	179.8	180.0	0.068	0.044
	CASSCF/cc-pVTZ	1.068	1.249	1.236	179.8	179.9	0.078	0.034
	CASSCF/ANO-L	1.068	1.250	1.233	179.6	179.9	0.085	0.004
	CCSD(T)/aug-cc-pCVQZ[b]	1.059	1.241	1.232				0.048
$1^3A''$	CASPT2/cc-pVTZ	1.107	1.464	1.230	106.0	129.1	3.007	2.943
	CASSCF/cc-pVTZ	1.132	1.487	1.223	104.9	129.9	3.006	2.944
	CASSCF/ANO-L	1.094	1.471	1.219	107.2	132.0	2.532	2.783
$1^1A''$	CASPT2/cc-pVTZ	1.108	1.447	1.228	105.6	130.4	3.353	3.296
	CASSCF/cc-pVTZ	1.104	1.479	1.231	105.2	130.7	3.233	3.346
	CASSCF/ANO-L	1.094	1.447	1.214	107.5	133.2	2.830	3.048
$1^3A'$	CASPT2/cc-pVTZ	1.071	1.352	1.266	134.9	125.2	3.573	3.487
	CASSCF/cc-pVTZ	1.070	1.378	1.261	132.4	128.0	3.561	3.490
	CASSCF/ANO-L	1.059	1.288	1.172	138.4	170.8	2.411	3.207

[a] The CASSCF and CASPT2 energies for the ground state of $HCCO^-$ are −151.3351298 and −151.7665375 au, −151.3357252 and −151.7659600 au, −151.3541311 and −151.8854333 au, respectively, at the levels of CASPT2/cc-pVTZ, CASSCF/cc-pVTZ and CASSCF/ANO-L

[b] The theoretical values were taken from Ref. [13]

respectively. Obviously, the transition from X^2A'' to $2^2\Pi$ ($2^2A''$) is the most intense among these transitions, and it is the only transition that has been detected up to now [7–10].

The CASPT2//CASPT2 T_0 values of *cis*-$1^4A''$, $1^4A''$, $1^4A'$, *cis*-$1^4A'$ and $2^4A''$ are 2.451, 2.757, 4.990, 5.720 and 6.086 eV, respectively. The energy gap (2.233 eV) between the $1^4A''$ state and the $1^4A'$ state suggests that the transition from 9a′ to 3a″ needs much energy than that from 9a′ to 10a′. The energy of *cis*-$1^4A''$ is lower by 0.306 eV than that of $1^4A''$, indicating that it is favorable to form the *cis*-$1^4A''$ state in the intersystem crossing (ISC) process [24].

3.2 $HCCO^-$

3.2.1 Geometries

As can be seen in Table 4, the ground state X^1A' of $HCCO^-$ has a *trans*-bent structure. Compared with the ground state of HCCO (Table 2), the 2a″ orbital of the X^1A' state of $HCCO^-$ is the double occupation as displayed in Table 5. The 2a″ orbital is a π* (π_{C1-C2}–Op_z) orbital. Therefore, the C–C bond length of the X^1A' state of $HCCO^-$ decreases to 1.260 Å and the C–O bond length increases to 1.227 Å, respectively. Similarly, compared with the $1^2\Pi$ ($1^2A'$) state of HCCO, the double occupation of the 9a′ orbital for the first low-lying excited state Σ^+ of $HCCO^-$ makes the C–C bond length decrease to 1.241 Å and the C–O bond length increase to 1.234 Å. Notably, these geometrical parameters of the X^1A' and Σ^+ states of $HCCO^-$ in our work are in good agreement with previous report at the CCSD(T)/aug-cc-pCVQZ level [13].

The $1^3A''$ and $1^1A''$ states come from the one electron transition from the 2a″ orbital to the 10a′ orbital, thus the two states possess similar geometrical structures as listed in

Table 5 Leading configurations (the weights exceed 0.05) and CI coefficients in the CASSCF calculations for the electronic states of $HCCO^-$[a]

State	Coef	Configuration
X^1A'	0.9516	$(8a')^2(1a'')^2(9a')^2(2a'')^2$
Σ^+	0.9548	$(1\pi_y)^2(1\pi_z)^2(2\pi_y)^2(2\pi_z)^2$
$1^3A''$	−0.9596	$(8a')^2(1a'')^2(9a')^2(2a'')^\alpha(10a')^\alpha$
$1^1A''$	−0.9604	$(8a')^2(1a'')^2(9a')^2(2a'')^\beta(10a')^\alpha$
$1^3A'$	0.9605	$(8a')^2(1a'')^2(9a')^\alpha(2a'')^2(10a')^\alpha$

[a] The common configuration (core)$(4a')^2(5a')^2(6a')^2(7a')^2$ is not presented for X^1A', $1^3A''$, $1^1A''$ and $1^3A'$. The configuration (core)$(4\sigma)^2(5\sigma)^2(6\sigma)^2(7\sigma)^2$ is not presented for Σ^+. In active orbitals the number '2' represents a fully occupied orbital, 'α' represents a singly occupied orbital containing an electron with an up spin, and 'β' represents a singly occupied orbital containing an electron with a down spin

Table 5. In detailed, the C–C bonds of the $1^3A''$ and $1^1A''$ states are elongated to 1.464 and 1.477 Å, respectively. The transition from 9a′ to 10a′ results in the formation of $1^3A'$, which makes the C–C and C–O bonds increase to 1.352 and 1.266 Å, respectively. Thus, the calculated geometry of $1^3A'$ at CASSCF/ANO-L level is abnormal in terms of the decrease of the C–O bond length.

In Table 6, we list the harmonic vibrational frequencies for the low-lying electronic states of $HCCO^-$. For the X^1A' state, it is found that the values of ν_1, ν_2, and ν_3 are close to those of the X^2A'' state of HCCO. Moreover, ν_4 increases to 612 cm^{-1}, while ν_5 decreases to 468 cm^{-1}. In the five states, only the Σ^+ state has two imaginary frequencies for the CCH bending modes, which has not been mentioned in previous studies. Thus, all states have stable structures except the Σ^+ state.

3.2.2 *The adiabatic excitation energies*

The difference of CASPT2//CASPT2 T_0 between X^1A' and Σ^+ is 0.044 eV (353 cm^{-1}), which is close to the reported energy barrier by Schäfer et al. (385 cm^{-1}) [13]. Moreover, it is observed that the values of CASPT2//CASPT2 T_0 for the $1^3A''$, $1^1A''$ and $1^3A'$ states are 2.943, 3.296 and 3.487 eV, respectively, as shown in Table 4. The T_0 value of the triplet state $1^3A''$ is lower by 0.353 eV than that of the singlet state $1^1A''$.

3.3 Detachment energy of $HCCO^-$

It can be seen from Table 7 that the first ADE and VDE of $HCCO^-$ are 2.210 and 2.362 eV, respectively, which are in agreement with experimental value of 2.338 ± 0.008 eV [13]. The ADE and VDE for the $1^2\Pi$ ($1^2A'$) state of the HCCO radical are 2.241 and 2.580 eV, respectively. Since the detachment energies of X^2A'' and $1^2\Pi$ ($1^2A'$) are close to each other, the $1^2\Pi$ ($1^2A'$) state will contribute to the neighborhood of 2.338 ± 0.008 eV in the experiment [13].

Though no experiments have reported that the detachment energies are larger than 3 eV, we predict the energy domain where the detachments of $HCCO^-$ occur. According to the Franck–Condon principle, we adopt the VDE values to assign the corresponding bands in the following discussion. The values of VDE for $1^4A''$, $2^2A'$ and $2^2\Pi$ ($2^2A''$) are 6.860, 6.693 and 6.905 eV, respectively, which are very close to each other. So, the three states are at the same band. Additionally, compared with the order of the VDE for $2^2A'$ and $2^2\Pi$ ($2^2A''$), the order of ADE is in reverse. The $1^4A'$ and $2^4A''$ states should be located at much higher energy bands, and their VDE values are 7.908 and 8.944 eV, respectively.

Table 6 Harmonic vibrational frequencies for the low-lying electronic states of $HCCO^-$ calculated with the optimized geometries at CASSCF/ANO-L level[a]

State	$\nu_1(a')$	$\nu_2(a')$	$\nu_3(a')$	$\nu_4(a')$	$\nu_5(a')$	$\nu_6(a'')$	$\nu_7(a'')$
X^1A'	3,203	2,027	1,204	612	468	578	
Σ^+	3,414	2,106	1,213	621	784i	568	391i
$1^3A''$	3,048	1,650	904	594	1,145	328	
$1^1A''$	3,043	1,688	988	577	1,127	819	
$1^3A'$	3,471	2,151	1,268	314	712	568	

[a] $\nu_1(a')$ denotes CH stretch, $\nu_2(a')$ denotes asymmetric CCO stretch, $\nu_3(a')$ denotes symmetric CCO stretch, $\nu_4(a')$ denotes CCO (*trans*) bending, $\nu_5(a')$ denotes CCH (*cis*) bending, $\nu_6(a'')$ denotes CCO out-of-plane bending, $\nu_7(a'')$ denotes CCH out-of-plane bending mode of the Σ^+ state

The harmonic vibrational frequencies are in cm^{-1}

Table 7 CASPT2 adiabatic and vertical detachment energies of $HCCO^-$ calculated with the optimized geometries of $HCCO^-$ at CASSCF/ANO-L level

State	ADE (eV)	VDE (eV)
X^2A''	2.210	2.362
$1^2\Pi$ ($1^2A'$)	2.241	2.580
$1^4A''$	5.014	6.860
$2^2A'$	6.294	6.693
$2^2\Pi$ ($2^2A''$)	6.207	6.905
$1^4A'$	7.189	7.908
$2^4A''$	8.376	8.944

4 Conclusions

In the present work, through the CASSCF and CASPT2 methods, we study the geometries, and the corresponding adiabatic excitation energies and the harmonic vibrational frequencies of the low-lying electronic states of the HCCO radical and its anion. By comparing the CASSCF and CASPT2 geometries, we found that the CASPT2 geometries are in better agreement with experimental values. For the X^2A'' state of HCCO, the calculated harmonic vibrational frequencies values of ν_1, ν_2, and ν_5 are close to experimental results. Moreover, one of the R–T pair $2^2A'$ is bent, while the other $2^2\Pi$ ($2^2A''$) is linear. Interestingly, the two states are found to be carbon-based radicals through the analyses of Mulliken spin populations, which are significantly different from previous report. The energy order of the two states is dependent on the employed basis sets. For $HCCO^-$, the first ADE and VDE are 2.210 and 2.362 eV, respectively, which well agree with the experiment of PES. According to the values of VDE, the next band of PES is predicted to be ~6.80 eV. Comparing with previous studies, we also study several higher excited states

of the HCCO radical ($1^4A'$, $2^4A''$ and *cis*-$1^4A'$) and its anion ($1^3A''$, $1^1A''$ and $1^3A'$). The present results might provide a theoretical guidance to further explore the absorption spectrum and the photoelectron spectrum of the HCCO radical and its anion.

References

1. Harding LB (1981) J Phys Chem 85:10
2. Michael JV, Wagner AF (1990) J Phys Chem 94:2453
3. Boullart W, Peeters J (1992) J Phys Chem 96:9810
4. Peeters J, Langhans I, Boullart W (1994) Int J Chem Kinet 26:869
5. Endo Y, Hirota E (1987) J Chem Phys 86:4319
6. Ohshima Y, Endo YJ (1993) Mol Spectrosc 159:458
7. Mordaunt DH, Osborn DL, Choi H, Bise RT, Neumark DM (1996) J Chem Phys 105:6078
8. Osborn DL, Mordaunt DH, Choi H, Bise RT, Neumark DM, Rohlfing CM (1997) J Chem Phys 106:10087
9. Brock LR, Mischler B, Rohlfing EA, Bise RT, Neumark DM (1997) J Chem Phys 107:665
10. Brock LR, Mischler B, Rohlfing EA (1999) J Chem Phys 110:6773
11. Wilhelm M, McNavage W, Groller R, Dai HL (2008) J Chem Phys 28:064313
12. Unfried KG, Glass GP, Curl RF (1991) Chem Phys Lett 177:33
13. Schäfer-Bung B, Engels B, Taylor TR, Neumark DM, Botschwina P, Peric M (2001) J Chem Phys 115:1777
14. Oakes JM, Jones ME, Bierbaum VM, Ellison GB (1983) J Phys Chem 87:4810
15. Herzberg G, Teller E (1933) Z Phys Chem Abt B 21:410
16. Renner R (1934) Z Phys Chem 92:172
17. Lee TJ, Fox DJ, Schaefer HF, Pitzer RM (1984) J Chem Phys 81:356
18. Szalay PG, Rogarasi G, Nemes L (1996) Chem Phys Lett 263:91
19. Schäfer B, Peric M, Engels B (1999) J Chem Phys 110:7802
20. Sattelmeyer KW, Yamaguchi Y, Schaefer HF (2004) Chem Phys Lett 383:266
21. Szalay PG, Tajti A, Stanton JF (2005) Mol Phys 103:2159
22. Jerosimić SV (2007) J Mol Spectrosc 242:139
23. Yamaguchi Y, Rienstra-Kiracofe JC, Stephens JC, Schaefer HF (1998) Chem Phys Lett 291:509
24. Hu CH, Schaefer HF, Hou Z, Bayes KD (1993) J Am Chem Soc 115:6904
25. Nguyen MT, Boullart W, Peeters J (1994) J Phys Chem 98:8030
26. Yarkony D (1996) J Phys Chem 100:17439
27. Wei ZZ, Li BT, Zhang HX (2007) J Comput Chem 28:467
28. Li BT, Wei ZZ, Zhang HX (2006) J Phys Chem A 110:10643
29. Hou CY, Zhang HX, Sun CC (2006) J Phys Chem A 110:10260
30. Serrano-Andrés L, Roos BO (1996) J Am Chem Soc 118:185
31. Pou-Amérigo R, Merchán M, Ortí E (1999) J Chem Phys 110:9536
32. Liu YJ, Huang MB (2002) Chem Phys Lett 360:400
33. Yu SY, Huang MB (2007) Chem Phys Lett 440:187
34. Malmqvist P-Å, Rendell A, Roos BO (1990) J Phys Chem 94:5477
35. Roos BO, Taylor PR, Siegbahn PEM (1980) Chem Phys 48:157
36. Andersson K, Malmqvist P-Å, Roos BO, Sadlej AJ, Wolinski K (1990) J Phys Chem 94:5483
37. Andersson K, Malmqvist P-Å, Roos BO (1992) J Chem Phys 96:1218
38. Dunning TH (1989) J Chem Phys 90:1007
39. Widmark P-O, Malmqvist P-Å, Roos BO (1990) Theor Chim Acta 77:291
40. Widmark P-O, Persson BJ, Roos BO (1991) Theor Chim Acta 77:419
41. Bernhardsson A, Lindh R, Olsen J, Fülscher M (1999) Mol Phys 96:617
42. Malmqvist P-Å, Roos BO (1989) Chem Phys Lett 155:189
43. Karlström G, Lindh R, Malmqvist P-Å, Roos BO, Ryde U, Veryazov V (2003) Comput Mater Sci 28:222